Nanoscale

Accepted Manuscript

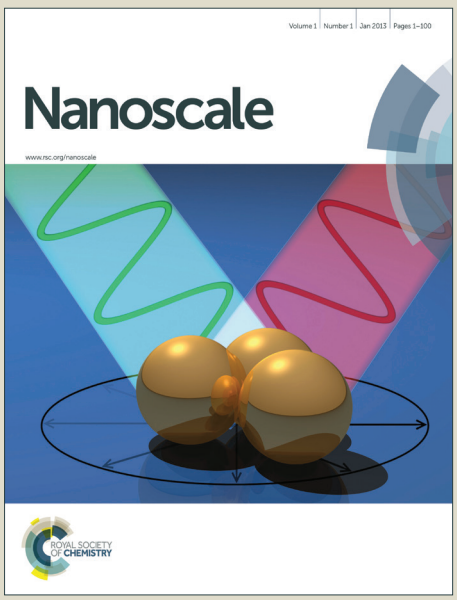

ROYAL SOCIETY OF CHEMISTRY

www.rsc.org/nanoscale

In-situ studies on controlling atomically-accurate formation process of gold nanoclusters

Lina Yang,[1†] Hao Cheng,[1†] Yong Jiang,[1] Ting Huang,[1] Jie Bao,[1] Zhihu Sun,[1]* Zheng Jiang,[2] Jingyuan Ma,[2] Fanfei Sun,[2] Qinghua Liu,[1] Tao Yao,[1]* Huijuan Deng,[3] Shuxin Wang,[3] Manzhou Zhu,[3] and Shiqiang Wei[1]*

[1]*National Synchrotron Radiation Laboratory, University of Science and Technology of China, Hefei 230029, P. R. China*
[2]*Shanghai Synchrotron Radiation Facility, Shanghai Institute of Applied Physics, Chinese Academy of Sciences, Shanghai 201204, P. R. China*
[3]*Department of Chemistry, Anhui University, Hefei 230039, P. R. China*

Abstract: Knowledge of the molecular formation mechanism of metal nanoclusters is essential for developing chemistry for accurate control over their synthesis. Herein, the "top-down" synthetic process of monodisperse Au_{13} nanoclusters via HCl etching polydisperse Au_n clusters ($15 \le n \le 65$) is traced by a combination of *in-situ* X-ray/UV-vis absorption spectroscopies and time-dependent mass spectrometry. It is revealed experimentally that the HCl-induced synthesis of Au_{13} is achieved by accurately controlling the etching process with two distinctive steps, in sharp contrast to the traditional thiol-etching mechanism through release of Au(I) complex. The first step involves the direct fragmentation of the initial larger Au_n clusters into metastable intermediate Au_8–Au_{13} smaller clusters. This is a critical step, which allows for the secondary size-growth step of the intermediates toward the atomically monodisperse Au_{13} clusters via incorporating the reactive Au(I)-Cl species in the solution. Such a secondary-growth pathway is further confirmed by the successful growth of Au_{13} through reaction of isolated Au_{11} clusters with $AuClPPh_3$ in the HCl environment. This work addresses the importance of reaction intermediates in guiding the way towards controllable synthesis of metal nanoclusters.

Keywords: monodisperse gold nanoclusters, etching mechanism, *in-situ* studies

† These authors contributed equally to this work.
* Corresponding authors. E-mail: zhsun@ustc.edu.cn; yaot@ustc.edu.cn; sqwei@ustc.edu.cn.

1. Introduction

Ultrasmall gold nanoclusters consisting of a few to tens of Au atoms have emerged as a new type of nanomaterials with diverse potential applications in catalysis, optical devices, imaging, and many others, oweing to their unique "superatom" structure, extraordinary stability and discrete electronic energy levels.[1-6] For both basic and application researches, the availability of well-defined nanoclusters is crucial, which depends critically on the design and implementation of solution-based synthetic chemistry. The most common top-down synthetic strategy of monodisperse Au nanoclusters is the size-focusing methodology that converts pre-formed polydisperse nanoclusters into monodisperse ones,[7] using a specific etchant such as thiol (SR), thiophenol or hydrochloric acid (HCl). Good examples of this methodology are Au_{25} nanorods converted from triphenylphosphine (PPh_3)-protected polydisperse Au nanoparticles (1–3.5 nm) via one-pot thiol etching,[8, 9] SR-protected Au_{38} etched from Glutathionate (SG)-protected Au_n ($38<n<102$)[10] or Au_n ($10<n<39$)[11] mixed clusters, thiophenol-stabilized Au_{36} clusters converted from Au_{68} and Au_{102} mixture,[12] and diphosphine-protected icosahedral Au_{13} clusters obtained through the HCl-etching of polydisperse Au_n clusters.[13-15] In spite of these great progresses, mechanistic insights into etching reaction still lag behind and remain a subject to be resolved.

The currently prevailing etching mechanism of Au clusters is obtained from SR-etching reactions. It assumes gradual release of Au(I) complexes[10,14-17] until the remaining cores reach a stable size in the etching environment (Path 1 in Fig. 1), a phenomenon known as the "survival of the most robust".[2, 7] For instance, the etching reaction of $Au_n(SG)_m$ clusters with free GSH under aerobic conditions converts $Au_n(SG)_m$ ($n\geq25$) clusters into $Au_{25}(SG)_{18}$ clusters, while $Au_n(SG)_m$ ($n<25$) clusters were completely dissolved into Au(I)-SG complexes.[16] As a result, the reaction yield is not very high (typically <25%).[10, 17] Other hypothesis involving direct depletion of the same-sized particle as the target cluster (Path 2 in Fig. 1) in a single etching step has also been proposed but not experimentally verified.[18] To obtain mechanistic insights into a practical etching reaction, determination of the reaction intermediates and their abundance is of paramount importance. From a more general aspect, the synthesis of nanoclusters usually involves the competitive etching and growth processes,[19, 20] and deliberate control over

this competition is essential for obtaining monodisperse atomically precise clusters. Undoubtedly, the details of etching reactions have significant influences on the design and attainment of nanoclusters (especially the reaction yield), as well as on tuning the compositions and properties of the end products. Such knowledge would offer great help to optimize the synthesis conditions and/or to develop more routes to "capture" the metastable species. This is a challenging task, the solution to which demands real-time studies on the reaction course at the atomic/molecular level, especially using a combination of various techniques affording complementary information from different aspects.

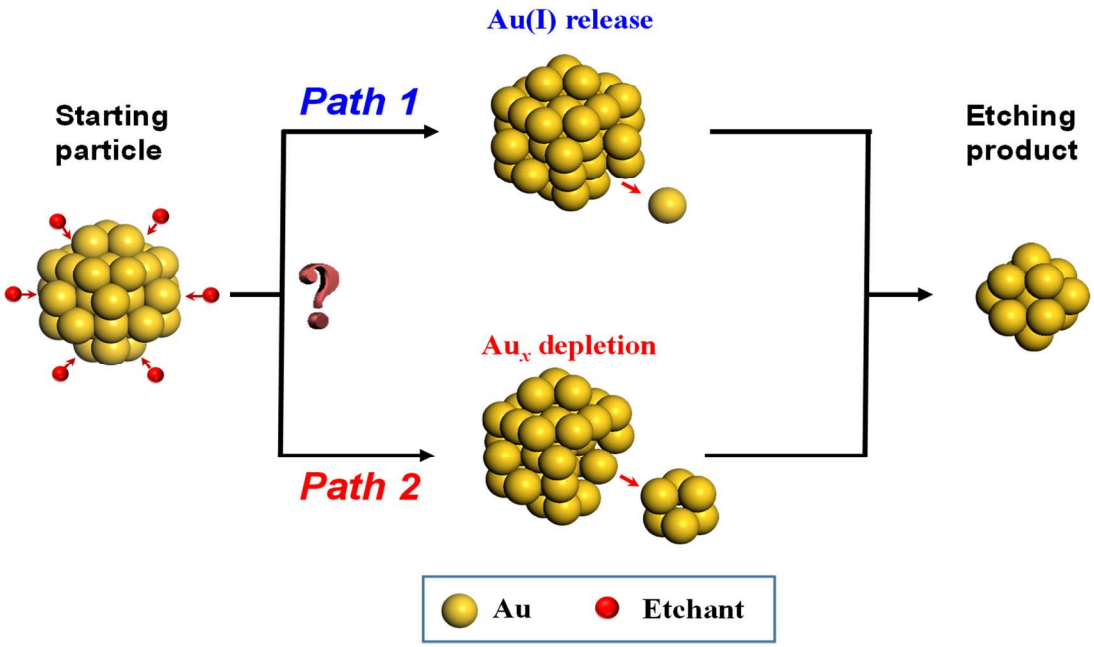

Figure 1. Schematic illustration of different etching reaction paths during the etching-induced syntheis of atomically precise metal nanoclusters.

Herein, we report a study on the top-down formation process of monodisperse $Au_{13}(L_3)_4Cl_4$ (L_3: 1,3-bis(diphenylphosphino)propane) nanoclusters converted from polydisperse precursor clusters via HCl etching,[14] by *in-situ* x-ray absorption fine structure (XAFS), UV-vis absorption in conjunction with *ex-situ* mass spectrometry. We chose this synthetic protocol as our target for studying the etching reaction process because it is a typical, well-controlled reaction for synthesizing Au_{13} cluster with an intriguingly high yield (>70%).[15] Such a high yield could hardly be understood by the conventional etching Path 1 where most of the Au atoms are wasted as Au(I) complex. To

unravel the HCl-etching path, particular emphasis will be given to detect reaction intermediates and analyze their evolution by a combination of *in-situ* XAFS and UV-vis absorption spectra, the validity of which has been proved by many previous studies of our group[21-26] and Tanaka group.[27, 28] An etching/growth manner including two distinctive reaction stages is observed, *i.e.*, the initial polydisperse Au_n ($15 \leq n \leq 65$) clusters are directly fragmented into Au_8–Au_{13} intermediate clusters, which then undergo a size-convergence process into uniform $Au_{13}(L_3)_4Cl_4$ clusters through incorporating the reactive Au(I)-Cl species in the solution.

2. Experimental Section

Sample preparations. The monodisperse $Au_{13}(L_3)_4Cl_4$ nanoclusters were synthesized by reaction of HCl with preformed L_3-capped Au_n clusters (Fig. S1(a)), following the protocol proposed by Shichiba *et al*.[14] but modified slightly. First, polydisperse L_3-protected Au_n clusters were synthesized by reduction of $Au_2(L_3)_2Cl_2$ (70 mg, 0.08 mmol) with $NaBH_4$ (15 mg, 0.4 mmol) in dichloromethane solvent. After removal of the solvent, the residue was filtered for several times to remove insoluble materials. The filtrate was evaporated to dryness (~ 19.5 mg) and then re-dissolved in 6 ml ethanol, acting as the starting material for the subsequent HCl-etching reaction. To this starting solution, 150 μL (1.8 mmol) HCl was added and drove the size-convergence process, during which the solution color gradually changed from dark brown to brownish orange. After stirring at room temperature for 10 h, the green solution was rotatory evaporated to dryness and then re-dissolved in 2 ml CH_2Cl_2. The mixture was poured into hexane (8 mL) and allowed to precipitate. The solid was collected by centrifugation (5 min, 14000 rpm) and washed with CH_2Cl_2/hexane (1:4, 10 mL) three times until ~12.6 mg of the end product was collected. The product yield could be roughly estimated by the mass ratio of the end product to the starting material, namely 12.6/19.5≈65%, in good agreement with the high yield (>70%) of monodisperse Au_{13} via HCl-etching as reported by Konish.[15] The obtained end product was subjected to subsequent measurements for identification.

***In-situ* XAFS and UV-Vis absorption measurements.** The Au L_3-edge XAFS spectra were measured at the BL14W1 beamline of the Shanghai Synchrotron Radiation Facility (SSRF) and the U7C beamline of National Synchrotron Radiation Laboratory

(NSRL). The storage ring of SSRF was operated at 3.5 GeV with a maximum current of 240 mA in the topup mode. The storage ring of NSRL was working at the energy of 0.8 GeV with a maximum electron current of 300 mA. Si(111) double-crystal monochromator crystals were used to monochromatize the X-ray beam. XAFS data were collected in transmission and quick-scan mode (1 min per scan) in the energy range from –200 below to 1000 eV above the Au L_3-edge. The reactive solution was continuously circulated along a microtube by peristaltic pump and flowed into a deliberately designed *in-situ* cell for simultaneous XAFS and UV−vis absorption measurement; the details of this setup have been described in our previous work.[24] The *in-situ* UV-Vis absorption spectra were recorded in transmission mode with the UV-vis light perpendicular to the incident X-ray beam. A TU-9001 spectrometer was used to collect the UV-vis data in the wavelength range of 250–800 nm, and the background absorption was corrected by pure ethanol.

Transmission electron microscopy (TEM) and matrix-assisted laser desorption ionization mass-spectrometry (MALDI-MS) measurements. TEM images were obtained with a JEM-2100F system. The samples for TEM were prepared by dropping the reaction solution onto copper TEM grids directly and drying in air. Mass spectra were measured with a Bruker Autoflex III mass spectrometer in positive linear mode. For minimization of fragmentation during lase desorption, trans-2-[3-(4-tert-butylphenyl)-2-methyl-2-propenyldidene] malononitrile (DCTB) was used as MALDI matrix and the laser pulse intensity was kept low enough for observation of the intact cluster ions. At a certain reaction time, aliquots were extracted from the reaction flask and then mixed with DCTB in the ratio of 1:1000. Then one or two microliters of the mixture was applied to the sample plate and air-dried for MS measurements performed within an m/z range from 2000 to 20000.

3. Results and Discussions

Shown in Fig. 2(a) and (b) are the time-dependent UV-vis absorption spectra and MALDI-MS during the synthesis of $Au_{13}(L_3)_4Cl_4$ nanoclusters (see Fig. S1 for the characterization) converted from L_3-protected Au_n mixture (Fig. S2). The inset in Fig. 2(a) shows the color of the solution at typical reaction times. For the starting material of

L_3-protected Au_n mixture prior to the HCl-etching reaction, the UV-vis absorption spectrum shows a featureless monotonous decrease, and MALDI-MS measurement shows a wide size range of 3000–13000 Da (Fig. 2(b)), corresponding to a crude mixture of Au_{15}–Au_{65}, in agreement with the polydispersity as seen by the TEM measurement (Fig. S2). At the reaction time of 1 h, there starts to appear a subtle UV-vis absorption peak at about 420 nm. This new absorption peak is originated from the L_3/Cl^--protected Au_8–Au_{13} clusters (especially Au_{11} clusters[29]) as observed by MALDI-MS, which display two regions covering roughly 3000–4000 Da (Au_8–Au_{13} clusters) and 6000–8000 Da (Au_{30}–Au_{40} mixtures), respectively (see Fig. S3 for the assignment of these mass peaks). At 2 h, a new absorption peak at around 340 nm is discernable, implying the gradually increased abundance of Au_{13} clusters, consistent with the MALDI-MS results. During this reaction stage, the larger Au_{30}–Au_{40} clusters vanish completely. As the reaction time reaches 4 h, both of the 340 and 420 nm absorption bands are distinct and the overall spectral shape resembles that of $Au_{13}(L_3)_4Cl_4$ nanoclusters.[14] Correspondingly, the cluster size range as indicated by MALDI-MS is narrowed to Au_{11}–Au_{13}, with $Au_{13}(L_3)_4Cl_4$ (m/z =4352.2 Da) peak being the dominant. From 4 h on, the relative abundance of Au_{13} is further increased at the cost of Au_{11}–Au_{12}. After a sufficiently long reaction (10 h), only the Au_{13} clusters are left, indicative of the formation of monodisperse Au_{13}. We note that the whole cluster conversion process in our case is considerably slower than that observed by Shichiba *et al.*'s,[14] possibly due to the lower content of HCl and the larger polydispersity of our starting material prepared by a slightly different method.

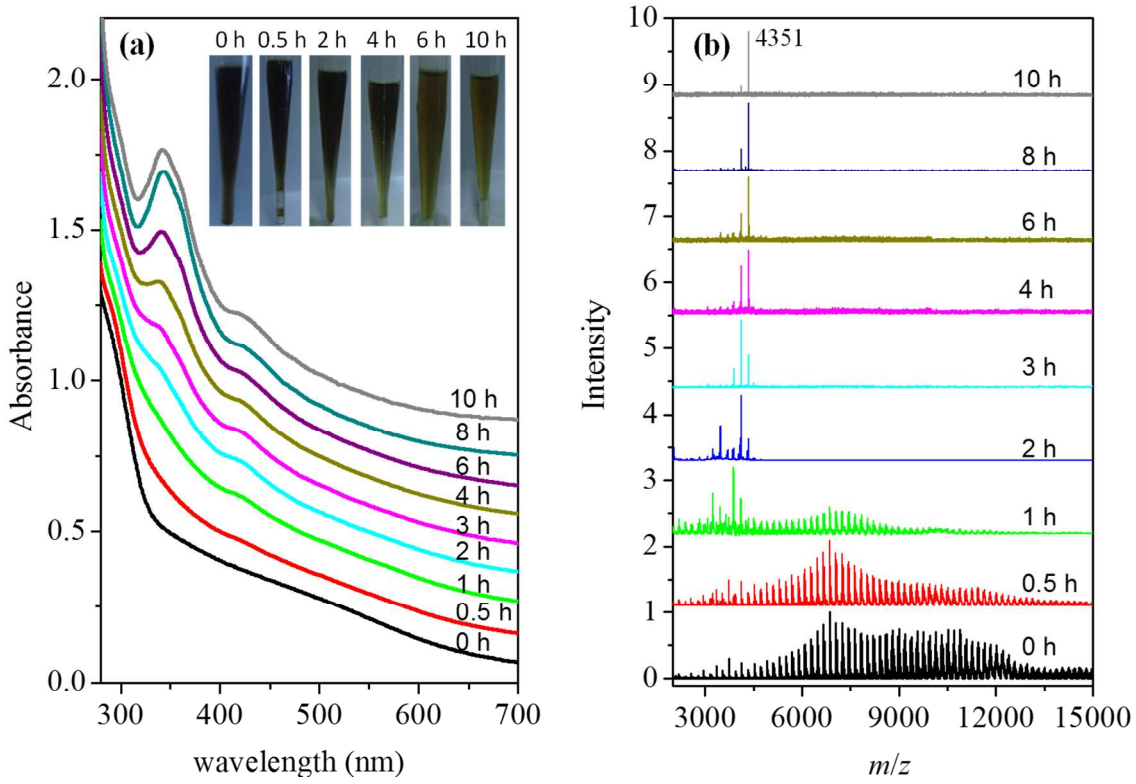

Figure 2. (a) *In-situ* UV-vis absorption spectra and (b) MALDI mass spectra against HCl-etching reaction times. The inset of (a) shows the solution color at typical reaction times.

The above UV-vis absorption and MALDI mass spectra have shown the formation and dissappeance of the intermediate Au_8–Au_{12} clusters, but they could hardly show how these intermediates are connected to the end product Au_{13}: Do they eventually convert to Au_{13} or dissolve into the solution as Au(I) complexes? To detect the fate of these intermediate species, we conducted *in-situ* XAFS measurements at Au L_3-edge in the whole size-conversion process. The time-dependent X-ray absorption near-edge structure (XANES) spectra (Fig. 3(a), shifted vertically for clarity) display the characteristic of face-centered-cubic (*fcc*) structured Au.[30, 31] The white-line peak at around 11926 eV, corresponding to the $2p_{3/2}\rightarrow 5d_{5/2,3/2}$ electronic transition of Au atoms, is strengthened immediately after addition of HCl (see Fig. S4(a) for the overlapped XANES spectra). This suggests the depletion of Au 5*d* electrons, most possibly due to the charge transfer from Au atoms to the Cl^- ligands. The Fourier transformed (FT) EXAFS k^2-weighted $\chi(k)$ functions shown in Fig. S5(a) are displayed in Fig. 3(b) (shifted vertically for clarity). It

shows that adding HCl intensifies the Au-ligand (Au−P/Cl, indistinguishable by EXAFS) peak at 1.90 Å, while damps the Au−Au peaks at 2.36 and 2.88 Å, suggesting the decomposition of the larger clusters. With prolonged reaction, these spectral changes continued but not as remarkably as those within the first 1 h (see Fig. S4(b)) for the overlapped EXAFS spectra). Least-squares EXAFS curve-fittings were performed to obtain the quantitative structural parameters around Au atoms during the whole process. The fitting included an Au−P/Cl, and two Au−Au pairs standing for the central-peripheral and peripheral-peripheral Au−Au bonds in an complete or incomplete icosahedron (labelled by Au−Au(c-p) and Au−Au(p-p), respectively). The details of the fitting are described in the Electronic Supplementary Information, and the fitting results are shown in Figure S5(b) and Table S1. The obtained coordination number (CN), bond distance (*R*) and Debye-Waller factor (σ^2) are shown in Fig. 3(c)-(e) as functions of time.

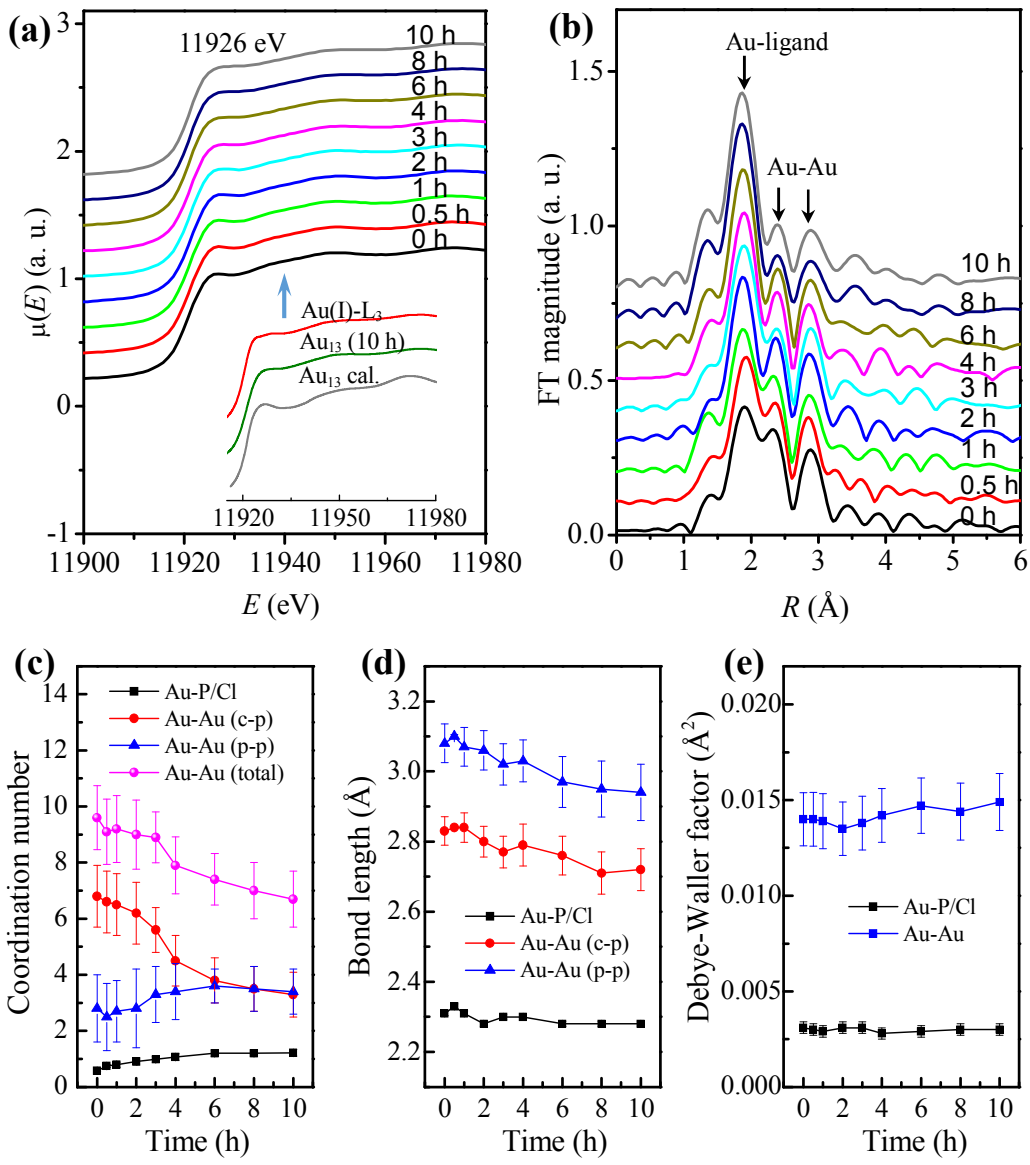

Figure 3. Time-dependent (a) XANES, and (b) EXAFS spectra. (c) Coordination number CN, (d) bond distance *R*, and (e) Debye-Waller factor σ^2 for the Au–P/Cl and Au–Au coordination pairs extracted from EXAFS curve-fitting against reaction time. Au–Au(c-p) and Au–Au(p-p) represent the central-peripheral and peripheral-peripheral Au–Au bonds in an complete or incomplete icosahedron, respectively. The inset in (a) compares the XANES spectrum for Au_{13} cluster at 10 h of HCl-etching time with that of Au(I)-L_3 species, and the calculated spectrum of the icosahedral $Au_{13}P_8Cl_4$ cluster.

From the time-evolutions of UV-vis absorption, XAFS, and mass spectra, the details of the formation process of $Au_{13}(L_3)_4Cl_4$ clusters could be inferred. Within the first etching stage of 2 h, the starting material of polydisperse Au_{15}–Au_{65} clusters are

prominently decomposed into smaller Au_8–Au_{13} intermediates. These Au_8–Au_{13} intermediates are most possibly fragmented from the larger Au_n ($15 \le n \le 65$) clusters, due to the interaction between H^+ and Au atoms at the surface of Au_n skeletons that are not fully protected by ligands, as suggested by the small Au-ligand CN of 0.58. To verify this point, we attempted parallel experiments using other protonic acids of sulfuric acid and acetic acid instead of HCl as etchants, which could also decompose the larger Au_n mixture (see Figs. S7 and S8 in the Electronic Supplementary Information). The fragmentation process can also be inferred by the decreased peripheral-peripheral Au–Au CN, as well as by the increased central-peripheral Au–Au CN in the first 2 h, since breaking larger cluster would yield more surface Au atoms to increase the peripheral-peripheral Au–Au CN (Fig. 3(c)). Immediately after their depletion, these active Au_8–Au_{13} clusters are stabilized by the quickly absorbed L_3 and Cl^- ligands to form metastable intermediates, as evidenced by the greatly enhanced Au–P/Cl coordination peak in the EXAFS-FT curve (Fig. 3(b)) and the remarkably increased Au–P/Cl CN (Fig. 3(c)). We note that at 2 h the clusters are nearly fully covered by ligands to form closed geometrical shells[16, 32, 33], for the Au–P/Cl CN (0.91) is very close to the nominal CNs of fully capped Au_8–Au_{13} clusters (ranging from 0.89 to 1.0, see Fig. S6 for their possible atomic structures).[34] The full protection of the intermediate clusters then prevents these Au_8–Au_{13} intermediates from further decomposing, which will be confirmed by our independent experiment demonstrating the unchanged Au_{11} in the HCl environment (*vide infra*). In the synthesis of Au nanoclusters via etching colloidal Au nanocrystals with polymers, Duan and Nie hypothesized a possible mechanism of liberation of the target Au_8 clusters but not confirmed;[18] our experimental observations then provide experimental evidence to this hypothesis. These etching-produced smaller intermediate clusters are quite essential intermediates, since they act as the seeds for the following size convergence toward stable monodisperse Au_{13} clusters.

The second stage (2–10 h) is mainly dominated by the size-focusing of these metastable Au_8–Au_{13} intermediates into Au_{13} cores in a secondary-growth manner, through incorporating the reactive Au(I)-Cl species in the solution. Such Au(I)-Cl species are possibly formed in the etching step, where a minority of Au atoms are inevitably

detached from the initial Au_n clusters as Au(I) ions and interact with Cl^- ions from HCl. To test that such a secondary-growth manner is possible, we also designed an additional experiment to grow isolated Au_{11} into Au_{13} clusters, through the reaction of Au_{11} with $AuClPPh_3$ in the HCl environment. The isolated Au_{11} cluster was synthesized using a conventional method (see details in the Electronic Supplementary Information).[29, 34-36] Mass spectra and *in-situ* UV-vis absorption spectra as shown in Fig. 4 (a) and (b) were conducted to identify the clusters and monitor their size change. Clearly, the evolutions of mass spectra and UV-Vis spectral features demonstrate that the reaction of $Au_{11}(L_3)_4Cl_2$ (m/z=3885) with $AuClPPh_3$ in the HCl environment can successfully grow $Au_{11}(L_3)_4Cl_2$ into $Au_{13}(L_3)_4Cl_4$ (m/z=4351), in perfect accord with the above proposed growth scenario. However, without the addition of HCl, the reaction of $Au_{11}(L_3)_4Cl_2$ with $AuClPPh_3$ alone did not lead to the formation of Au_{13} clusters within 24 h. This suggests that HCl still plays important roles in the secondary-growth stage, presumably because the significantly increased content of reactive Cl^- enhances the reactivity of the AuCl species in solution and promotes the cluster growth. Besides, we also tested that if $AuClPPh_3$ was not added, the UV-vis spectral features of $Au_{11}(L_3)_4Cl_2$ do not change after a sufficiently long time (> 8 h) of stirring in the HCl environment, demonstrating the resistance of $Au_{11}(L_3)_4Cl_2$ to HCl etching.

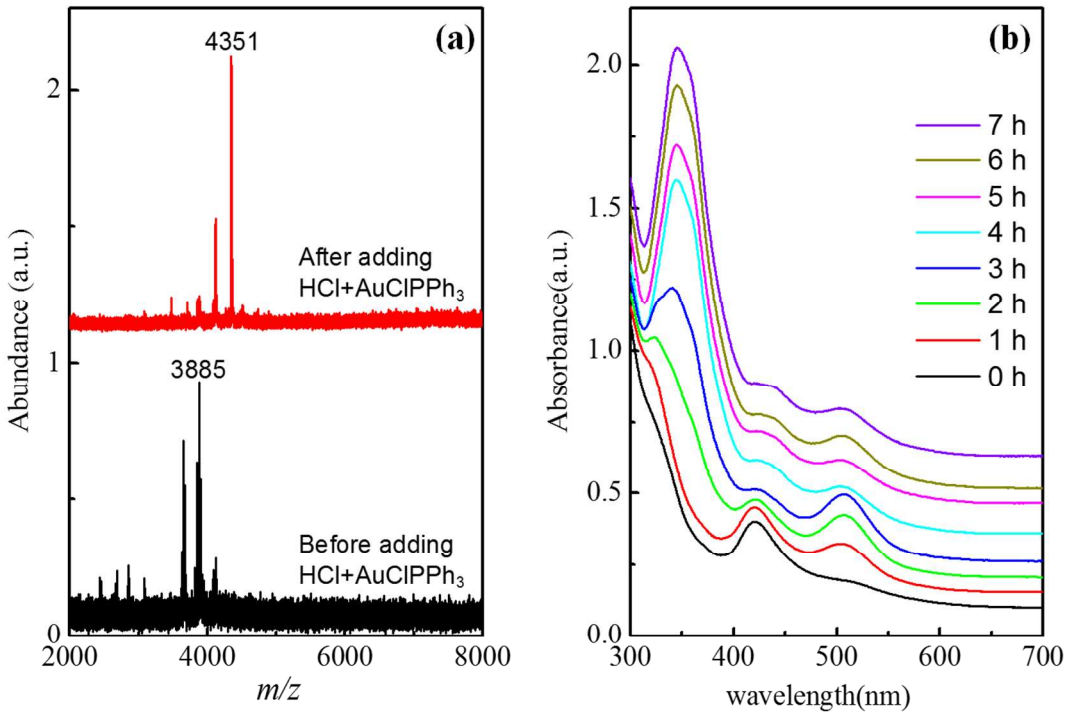

Figure 4. (a) MALDI mass spectra of Au_{11} clusters before and after adding HCl+AuClPPh$_3$. The peaks at *m*/*z*=3885 and 4351 are corresponding to $Au_{11}(L_3)_4Cl_2$ and $Au_{13}(L_3)_4Cl_4$, clusters, respectively. (b) *In-situ* UV-vis absorption spectra for the conversion of Au_{11} into Au_{13} clusters.

More evidence to this secondary-growth manner could be found from in-depth analysis of the XAFS spectra. We compare in the inset of Fig. 3(a) the XANES spectrum at the reaction time of 10 h with the spectrum of Au(I)-L_3 species and the calculated spectrum of a $Au_{13}P_8Cl_4$ cluster in the icosahedral configuration[34] using the *ab initio* multiple-scattering code FEFF8.20.[37] Evidently, the experimental spectral features at 10 h could be well reproduced by the calculation for the $Au_{13}P_8Cl_4$ cluster, but they are remarkably different from those of Au(I)-L_3 species which show a double-peak structure in the white-line region. More quantitative results could be obtained from EXAFS analysis. At 10 h the Au-ligand CN (1.21) is between the nominal values in $Au_{13}(L_3)_4Cl_4$ (0.92) and Au(I)-L_3 species or analogues (2.0),[34, 38] suggesting the coexistence of both species. The real Au-ligand CN could be expressed as a weighted-sum of the CNs in $Au_{13}(L_3)_4Cl_4$ and Au(I)-L_3 *via* $0.92\times p+2\times(1-p)=1.21$, which gives the proportion p of Au atoms in $Au_{13}(L_3)_4Cl_4$ as $p\sim0.7$. Therefore, after 10 h of reaction, the majority (~70%) of

Au atoms are in the form of Au_{13} cluster, with a small part (~30%) existing as Au(I)-L_3 species or analogues. This result is close to the reaction yield (~65%) estimated from the mass ratio of the starting material (~19.5 mg) and end product (~12.6 mg), in good agreement with the yield of 70% for the HCl-etching protocol.[15]

The growth of the Au_8–Au_{12} intermediates into the Au_{13} clusters is possibly driven by the geometric factor, *i.e.*, the incomplete icosahedral structures of these intermediate clusters are prone to convert into the close structure of complete icosahedral Au_{13} clusters, in the presence of reactive AuCl species.[15] Indeed, such a AuCl- or even Cl^--assisted growth manner has been used in the high-yield synthesis of numerous Au clusters. For example, in the presence of Cl^- with coordinating capability, Vollenbroek *et al*.[39] and Briant *et al*.[40] reported the synthesis of $[Au_{13}(PMe_2Ph)_{10}Cl_2]^{3+}$ and $[Au_{11}(PPh_3)_8Cl_2]^+$ clusters converted from $[Au_{11}(PMe_2Ph)_{10}]^{3+}$ and $[Au_9(PPh_3)_8]^{3+}$, respectively. Similarly, $[Au_8(L_3)_4Cl_2]^{2+}$ [35] and $[Au_{11}(PPh_3)(L_5)_4Cl]^{2+}$ (L_5: Ph_2P-$(CH_2)_5$-PPh_2)[41] clusters could also be readily grown through a reaction of $[Au_6(L_3)_4]^{2+}$ and $[Au_{10}(L_5)_4]^{2+}$ primary clusters with the Au(I)-Cl complex $AuClPPh_3$, respectively.

Concluding the above results, we could draw a clear picture on the formation process of Au_{13} clusters converted from polydisperse mixtures via HCl-etching. This process could be roughly divided into two distinct etching/growth stages as schematically shown in Fig. 5. Within the first 2 h, the most significant change is the decomposition of the crude Au_{15}–Au_{65} mixture into smaller Au_8–Au_{13} metastable intermediates. At further prolonged reaction time, the abundances of Au_8–Au_{12} decrease steadily and Au_{13} becomes the most abundant cluster until nearly atomically monodisperse Au_{13} clusters are produced. Interestingly, this manner leads to a high-yield of the end product, in sharp contrast to the low-yield of the thiol-etching cases in which a large portion of excess Au atoms are dissolved as Au(I)-SR species and wasted.[10, 15, 42-44]

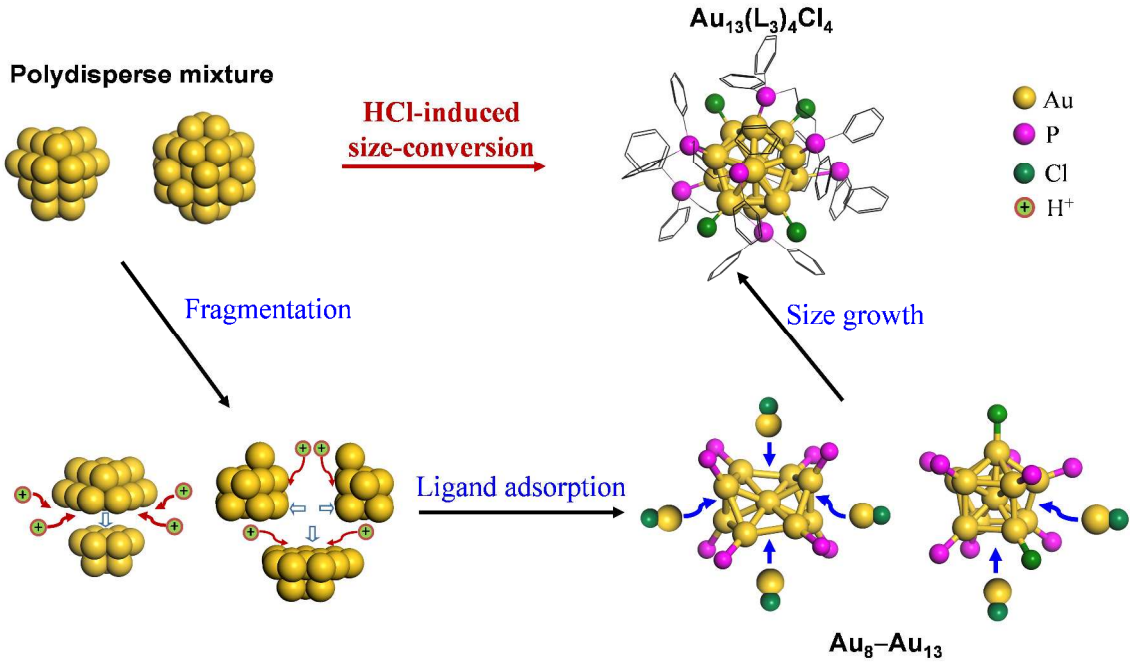

Figure 5. Schematic illustration of the HCl-induced conversion of polydisperse Au_n mixture into monodisperse $Au_{13}(L_3)_4Cl_4$ nanoclusters.

4. Conclusion

In summary, *in-situ* UV-vis/ XAFS and mass spectra are combined to probe the formation process of monodisperse $Au_{13}(L_3)_4Cl_4$ nanoclusters converted from polydisperse Au_n clusters. It is found that the cluster formation is achieved in an etching/growth manner including two distinct reaction steps. (1) The initial polydisperse Au_n ($15 \le n \le 65$) clusters are etched by HCl to form much smaller Au_8–Au_{13} intermediate clusters protected by L_3 and Cl^- ligands. (2) These intermediate species undergo a secondary-growth step to form uniform $Au_{13}(L_3)_4Cl_4$ clusters, by incorporating the reactive Au(I)-Cl species in the solution. Due to the secondary-growth step, the obtained monodisperse end product has a very high yield (~70%) relative to the polydisperse starting material, in sharp contrast to the low-yield of the thiol-etching cases where a large portion of Au atoms are wasted. These findings enrich our understanding on the etching mechanism during nanoclusters formation and can guide our way towards the design and synthesis of nanomaterials in a controllable manner.

Electronic Supplementary Information Synthesis and characterization of the

starting and end Au nanoclusters, assignment of the MALDI-MS peaks, details for the EXAFS curve-fitting and fitting results, parallel experiments using sulfuric acid and acetic acid as etchants, and experimental details for growing isolated Au_{11} into Au_{13} clusters in the HCl environment.

Notes

The authors declare no competing financial interest.

Acknowledgements

This work was supported by National Natural Science Foundation of China (Grant No. 11175184, 11135008, 11475176, 11422547, 11435012, 21471143 and U1332131), and the Foundation for Innovative Research Groups of the National Natural Science Foundation of China (11321503). The authors are grateful to NSRL and SSRF for the valuable synchrotron radiation XAFS beamtime.

References

1. R. C. Jin, *Nanoscale*, 2010, **2**, 343-362.
2. G. Li and R. C. Jin, *Acc. Chem. Res.*, 2013, **46**, 1749-1758.
3. H. F. Qian, M. Z. Zhu, Z. K. Wu and R. C. Jin, *Acc. Chem. Res.*, 2012, **45**, 1470-1479.
4. S. H. Yau, O. Varnavski and T. Goodson, *Acc. Chem. Res.*, 2013, **46**, 1506-1516.
5. Y. Z. Lu and W. Chen, *Chem. Soc. Rev.*, 2012, **41**, 3594-3623.
6. J. J. Spivey, K. S. Krishna, C. Kumar, K. M. Dooley, J. C. Flake, L. H. Haber, Y. Xu, M. J. Janik, S. B. Sinnott, Y. T. Cheng, T. Liang, D. S. Sholl, T. A. Manz, U. Diebold, G. S. Parkinson, D. A. Bruce and P. de Jongh, *J. Phys. Chem. C*, 2014, **118**, 20043-20069.
7. R. C. Jin, H. F. Qian, Z. K. Wu, Y. Zhu, M. Z. Zhu, A. Mohanty and N. Garg, *J. Phys. Chem. Lett.*, 2010, **1**, 2903-2910.
8. H. F. Qian, M. Z. Zhu, E. Lanni, Y. Zhu, M. E. Bier and R. C. Jin, *J. Phys. Chem. C*, 2009, **113**, 17599-17603.
9. H. F. Qian, W. T. Eckenhoff, M. E. Bier, T. Pintauer and R. C. Jin, *Inorg. Chem.*, 2011, **50**, 10735-10739.
10. H. F. Qian, Y. Zhu and R. C. Jin, *Acs Nano*, 2009, **3**, 3795-3803.
11. H. F. Qian, M. Z. Zhu, U. N. Andersen and R. C. Jin, *J. Phys. Chem. A*, 2009, **113**, 4281-4284.
12. P. R. Nimmala and A. Dass, *J. Am. Chem. Soc.*, 2011, **133**, 9175-9177.
13. Y. Shichibu and K. Konishi, *Small*, 2010, **6**, 1216-1220.
14. Y. Shichibu, K. Suzuki and K. Konishi, *Nanoscale*, 2012, **4**, 4125-4129.
15. Y. Shichibu, Y. Negishi, H. Tsunoyama, M. Kanehara, T. Teranishi and T. Tsukuda, *Small*, 2007, **3**, 835-839.
16. C. Kumara, V. R. Jupally and A. Dass, in *Gold Clusters, Colloids and Nanoparticles I*, ed. D. M. P. Mingos, Springer Int Publishing Ag, Cham, 2014, vol. 161, pp. 155-187.
17. H. W. Duan and S. M. Nie, *J. Am. Chem. Soc.*, 2007, **129**, 2412-+.

18. X. Yuan, B. Zhang, Z. T. Luo, Q. F. Yao, D. T. Leong, N. Yan and J. P. Xie, *Angew. Chem. Int. Ed.*, 2014, **53**, 4623-4627.
19. Z. T. Luo, V. Nachammai, B. Zhang, N. Yan, D. T. Leong, D. E. Jiang and J. P. Xie, *J. Am. Chem. Soc.*, 2014, **136**, 10577-10580.
20. K. Konishi, *Struct. Bond.*, 2014, **161**, 49-86.
21. Z. H. Sun, H. Oyanagi, M. Uehara, H. Nakamura, K. Yamashita, A. Fukano and H. Maeda, *J. Phys. Chem. C*, 2009, **113**, 18608-18613.
22. Z. H. Sun, H. Oyanagi, H. Nakamura, Y. Jiang, L. Zhang, M. Uehara, K. Yamashita, A. Fukano and H. Maeda, *J. Phys. Chem. C*, 2010, **114**, 10126-10131.
23. T. Yao, Z. H. Sun, Y. Y. Li, Z. Y. Pan, H. Wei, Y. Xie, M. Nomura, Y. Niwa, W. S. Yan, Z. Y. Wu, Y. Jiang, Q. H. Liu and S. Q. Wei, *J. Am. Chem. Soc.*, 2010, **132**, 7696-7701.
24. T. Yao, S. J. Liu, Z. H. Sun, Y. Y. Li, S. He, H. Cheng, Y. Xie, Q. H. Liu, Y. Jiang, Z. Y. Wu, Z. Y. Pan, W. S. Yan and S. Q. Wei, *J. Am. Chem. Soc.*, 2012, **134**, 9410-9416.
25. Y. Y. Li, H. Cheng, T. Yao, Z. H. Sun, W. S. Yan, Y. Jiang, Y. Xie, Y. F. Sun, Y. Y. Huang, S. J. Liu, J. Zhang, Y. N. Xie, T. D. Hu, L. N. Yang, Z. Y. Wu and S. Q. Wei, *J. Am. Chem. Soc.*, 2012, **134**, 17997-18003.
26. Y. Y. Li, S. J. Liu, T. Yao, Z. H. Sun, Z. Jiang, Y. Y. Huang, H. Cheng, Y. Y. Huang, Y. Jiang, Z. Xie, G. Q. Pan, W. S. Yan and S. Q. Wei, *Dalton Trans.*, 2012, **41**, 11725-11730.
27. T. Tanaka, J. Ohyama, K. Teramura and Y. Hitomi, *Catal. Today*, 2012, **183**, 108-118.
28. J. Ohyama, K. Teramura, Y. Higuchi, T. Shishido, Y. Hitomi, K. Kato, H. Tanida, T. Uruga and T. Tanaka, *Chemphyschem*, 2011, **12**, 127-131.
29. M. F. Bertino, Z. M. Sun, R. Zhang and L. S. Wang, *J. Phys. Chem. B*, 2006, **110**, 21416-21418.
30. P. Zhang and T. K. Sham, *Phys. Rev. Lett.*, 2003, **90**, 245502.
31. R. C. Jin, Y. Zhu and H. F. Qian, *Chem.-Eur. J.*, 2011, **17**, 6584-6593.
32. H. G. Boyen, G. Kastle, F. Weigl, B. Koslowski, C. Dietrich, P. Ziemann, J. P. Spatz, S. Riethmuller, C. Hartmann, M. Moller, G. Schmid, M. G. Garnier and P. Oelhafen, *Science*, 2002, **297**, 1533-1536.
33. J. I. Nishigaki, R. Tsunoyama, H. Tsunoyama, N. Ichikuni, S. Yamazoe, Y. Negishi, M. Ito, T. Matsuo, K. Tamao and T. Tsukuda, *J. Am. Chem. Soc.*, 2012, **134**, 14295-14297.
34. K. P. Hall and D. M. P. Mingos, *Prog. Inorg. Chem.*, 1984, **32**, 237-325.
35. Y. Kamei, Y. Shichibu and K. Konishi, *Angew. Chem. Int. Ed.*, 2011, **50**, 7442-7445.
36. J. M. M. Smits, J. J. Bour, F. A. Vollenbroek and P. T. Beurskens, *Journal of Crystallographic and Spectroscopic Research*, 1983, **13**, 355-363.
37. A. L. Ankudinov, B. Ravel, J. J. Rehr and S. D. Conradson, *Phys. Rev. B*, 1998, **58**, 7565-7576.
38. J. M. Pettibone and J. W. Hudgens, *Small*, 2012, **8**, 715-725.
39. F. A. Vollenbroek, J. J. Bour, J. M. Trooster and J. W. A. Vandervelden, *Journal of the Chemical Society-Chemical Communications*, 1978, DOI: Doi 10.1039/C39780000907, 907-909.
40. C. E. Briant, B. R. C. Theobald, J. W. White, L. K. Bell and D. M. P. Mingos, *Journal of the Chemical Society-Chemical Communications*, 1981, DOI: Doi 10.1039/C39810000201, 201-202.
41. J. M. Pettibone and J. W. Hudgens, *Phys. Chem. Chem. Phys.*, 2012, **14**, 4142-4154.
42. T. G. Schaaff and R. L. Whetten, *J. Phys. Chem. B*, 1999, **103**, 9394-9396.
43. G. H. Woehrle, L. O. Brown and J. E. Hutchison, *J. Am. Chem. Soc.*, 2005, **127**, 2172-2183.
44. J. P. Wilcoxon and P. Provencio, *J. Phys. Chem. B*, 2003, **107**, 12949-12957.